GaAs{001}(2×4) surface-structure studies with shadow-cone-enhanced secondary-ion mass spectrometry

C. Xu, K. P. Caffey, J. S. Burnham, S. H. Goss, B. J. Garrison, and N. Winograd
Department of Chemistry, The Pennsylvania State University, 152 Davey Laboratory, University Park, Pennsylvania 16802
(Received 13 September 1991; revised manuscript received 2 December 1991)

The atomic geometry of the GaAs{001}(2×4) surface has been analyzed quantitatively by shadow-cone-enhanced secondary-ion mass spectrometry. The technique is based on the concept that the shadow cone created by the interaction between an incident-ion beam and a surface atom focuses ion flux onto specific crystal coordinates. In this experiment, secondary Ga^+ ions were desorbed by a 3-keV Ar^+-ion beam and were detected at an energy of 20 eV. The surface was prepared by molecular-beam epitaxy and transferred *in situ* to an UHV surface-analysis chamber. The microscopic mechanisms of the desorption process were elucidated by a three-dimensional molecular-dynamics computer simulation. The data analysis also involved comparing the incidence angles corresponding to enhanced intensity features in the secondary-Ga^+-ion yield with the angles determined in a two-body-interaction calculation using the Molière approximation to the Thomas-Fermi potential. This study confirms the As_2-dimer structure of the GaAs{001}(2×4) surface, and the As-As bond length is determined to be 2.73±0.10 Å. This value suggests that, analogous to the atoms in bulk As, the As_2-dimer atoms are threefold coordinated. Within the precision of the analysis, no relaxations were observed in the second and deeper layers of the surface.

I. INTRODUCTION

The GaAs{001} surface is the most commonly used substrate in III-V compound semiconductor device applications, especially those which require film growth by molecular-beam epitaxy (MBE). Information about the atomic structure of GaAs{001} is extremely useful in determining the origin of surface electronic states, as revealed by photoemission spectroscopy,[1] and the relationship of these states to device performance. A better understanding of the surface geometry would prove helpful in modeling MBE growth and subsequent Schottky-barrier formation in compound semiconductor films.[2–5] Yet despite its technological relevance, little is known about the atomic structure of the GaAs{001} surface. One reason for this lack of data is that GaAs{001} displays a plethora of different reconstructions, depending on the [As]/[Ga] ratio.[6–8]

In terms of atomic geometry, the (2×4) reconstruction is the best understood GaAs{001} surface. In the early 1980s, a large number of Auger and photoemission studies demonstrated that the As coverage of the (2×4) reconstruction was in the range of 0.6–0.9 monolayer (ML).[1,9–12] This knowledge, in combination with the 2×4 periodicity of the surface, provided a framework of parameters within which theoreticians could perform total-energy calculations of the system in order to propose possible structures.[13,14] Scanning tunneling microscopy (STM) experiments eventually confirmed one of the proposed structures, resulting in the currently accepted model of the GaAs{001}(2×4) surface: the 2× periodicity in the $\langle 01\bar{1} \rangle$ crystal direction is caused by As_2 dimer formation, and the 4× periodicity in the $\langle 011 \rangle$ crystal direction occurs because every fourth As_2 dimer is missing from the surface.[3] This configuration corresponds to an As coverage of 0.75 ML. Very recently, x-ray photoelectron diffraction studies of the surface determined that the As-As bond distance is in the range 2.2–2.36 Å, depending upon whether a buckled geometry of the dimer is assumed, relative to the surface plane.[15] The STM experiments indicate that the $c(4\times4)$ reconstruction of GaAs{001} is also composed of As_2 dimers on the surface,[16] and x-ray scattering studies of this reconstruction indicate that the As-As bond length is 2.59±0.06 Å.[17,18]

Ion-scattering techniques have been used successfully during the last decade to elucidate the structure of surface phenomena such as relaxation and reconstruction.[19] Among the variety of methods used in ion-scattering studies, the shadowing effect has played an important role. When an ion beam impinges on an atom, this atom will cast a shadow of zero ion flux along the incident beam direction because of the repulsive atom-ion interaction. At the edge of this "shadow cone," the ion flux increases due to focusing: the so-called ion-focusing or wedge-focusing effect.[20,21] Since the dimensions of a shadow cone can be accurately calculated by using the Molière approximation to the Thomas-Fermi potential, this ion-focusing effect can be conveniently used in surface structure analysis.[22]

One application of the ion-focusing effect is the shadow-cone-enhanced secondary-ion mass spectrometry (SIMS) experiment.[23] In this technique, desorbed secondary ions are detected as a function of incident-ion polar angle. When an energetic ion beam impinges on a crystal surface, the ions transfer their momentum to the crystal during the atom-ion and atom-atom interactions. As a result, some atoms are ejected from the surface, and a fraction of these may be ionized. Although the process is

complicated, it has been discovered that a dramatic enhancement of the secondary-ion intensity is related to interactions of the shadow-cone tail of the primary ion beam with surface atoms. This interpretation is supported by molecular-dynamics calculations.[24–28] From the desorbed secondary-ion spectrum, the critical angle where the shadow-cone edge from one surface atom intersects a neighboring atom can be determined. Combined with the known shadow-cone shape, the surface structure can be extracted.

The shadow-cone-enhanced SIMS technique has been successfully employed in analyzing the surface structure of a metal, with and without the presence of an adsorbate.[27,29,30] Recently, this technique has been used in a semiconductor surface study to determine the chain-rotation structure of the GaAs{110} surface.[31] In this report we present a shadow-cone-enhanced SIMS study of the atomic geometry of the MBE-grown GaAs{001}(2×4) surface. The As-As bond distance is determined to be 2.73±0.10 Å. The experimental results are supported by molecular-dynamics simulations of energetic ion interactions with semiconductor surfaces.

II. EXPERIMENT

Descriptions of the apparatus and the crystal preparation have been published previously,[31–33] and so only a few details specific to this experiment will be discussed here. The angular definitions pertaining to the experiment are shown in Fig. 1. The azimuthal angle ϕ is defined in the plane of the crystal. The polar angle of incidence θ_i is defined as the angle between the surface normal and the ion beam. The detection angle β is defined as the angle between the ion beam and the entrance aperture of the detector. In a typical shadow-cone-enhanced SIMS experiment, the sample is aligned with a major crystallographic axis parallel to the plane of ion detection. In the case of the GaAs{001} surface we choose either the ⟨011⟩ or ⟨01$\bar{1}$⟩ direction. The data collection may then proceed in one of two methods. In the first method, the signal intensity of the secondary Ga^+ ions is measured as a function of the polar angle of incidence while the detection angle remains constant. In the second method, the polar angle of incidence is stepped while the angle of the detector relative to the surface normal, θ_d, remains constant.

The desorption process was initiated by a 3-keV Ar^+-ion beam. The ion beam was focused to a 2-mm-diameter-spot size and operated at a beam current in the 3–5-nA range. A typical experiment required about 10 min, and the sample position was stepped in the vertical axis after every measurement over a 40-mm range of the surface. The maximum ion flux during the experiment was therefore 2.3×10^{13} ions/cm^2, or 3.7% relative to the surface site density of GaAs{001} (6.26×10^{14} atoms/cm^2). This dose is safely within the static SIMS regime.

III. RESULTS AND DISCUSSION

A. The model GaAs{001}(2×4) surface

The currently favored model of the GaAs{001}(2×4) surface is shown in Fig. 2. Cross sections of the model surface, in planes which are perpendicular to the crystal face, are presented in Fig. 3(a) for the ⟨011⟩ direction and Fig. 3(b) for the ⟨01$\bar{1}$⟩ direction. In these figures the surface is represented by the first layer, and layers 2, 3, etc. designate layers that are deeper into the crystal. Both of the major crystallographic axes contain two planes which are nonequivalent, and the analysis of the shadow-cone-enhanced SIMS spectra must take each plane into consideration. Note that for the cross sections taken parallel to the ⟨011⟩ crystal direction, the two planes look very similar. What makes them unique is that in plane A of Fig. 3(a), the top-layer As is not coplanar with the second-layer Ga because the As atoms dimerize,

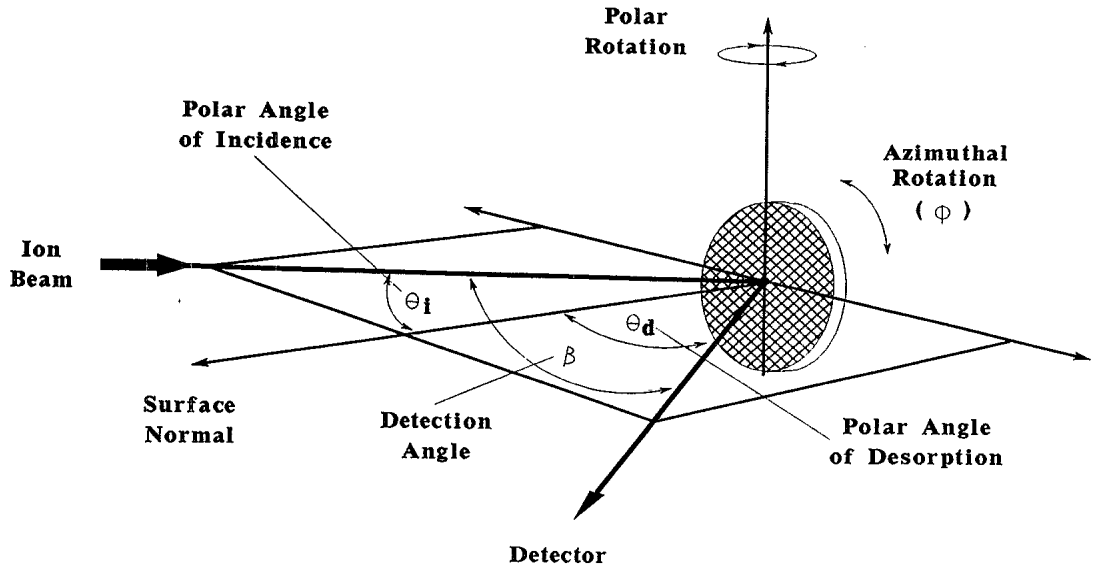

FIG. 1. A schematic of the angular definitions used in shadow-cone-enhanced SIMS experiments.

moving the As atom in the direction perpendicular to the plane of the figure. On the other hand, in plane B of Fig. 3(a), the third-layer As and fourth-layer Ga atoms are assumed to be coplanar. The two planes parallel to the $\langle 01\bar{1} \rangle$ direction in Fig. 3(b) are obviously very different.

An important consideration is whether the ion-atom shadow cone of one plane can interact with atoms in an adjacent plane. In the case of the GaAs{001}(2×4) surface, the planes are 2.0 Å apart. This spacing is large in comparison to the diameter of a shadow cone which results from the interaction of a 3-keV Ar^+-ion beam with the surface atoms. The maximum radius of shadow cones in these experiments was 1.5 Å. Therefore, the ion-atom interactions possible for each plane may be treated independently in the analysis.

B. Molecular-dynamics simulations

In order to elucidate the dynamics of the ion-atom and atom-atom collision events, and to predict the microscopic mechanisms of the desorption process, a three-dimensional molecular-dynamics calculation has been used in this study.[24] The results from the calculation were compared with the experimental distributions to verify the assignment of mechanisms responsible for the features of the spectra. Ideally, it is desirable to use the GaAs system in the simulation. Unfortunately, a well-tested interaction potential in the energy range of interest is not yet available for GaAs.

In contrast, the interaction potentials necessary to describe the bonding in Si have been well developed. It is possible to use a Si potential as a model since the bulk crystal structures of Si and GaAs are closely related, and since the response of a solid to keV-ion bombardment is influenced more strongly by structure than by chemical bonding forces. Moreover, there have been recent calculations for the angular distributions of Si atoms ejected from Si{110} and Si{001}(2×4) surfaces which are in good agreement with experimental Ga^+-ion distributions desorbed from the corresponding GaAs surfaces.[24,33] The calculation was therefore carried out with 3-keV

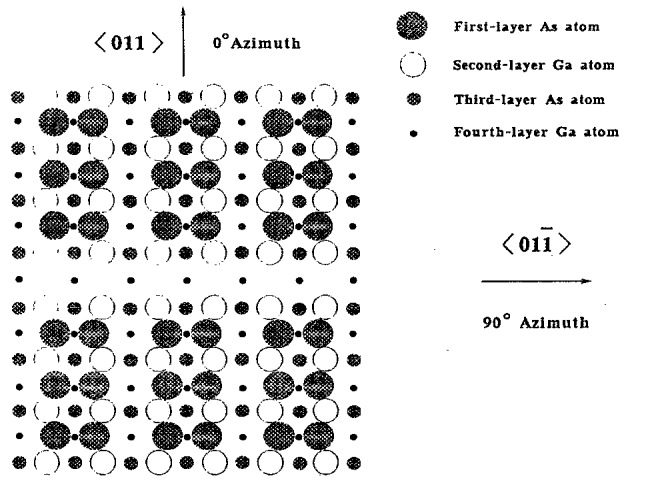

FIG. 2. A schematic of the GaAs{001}(2×4) model surface.

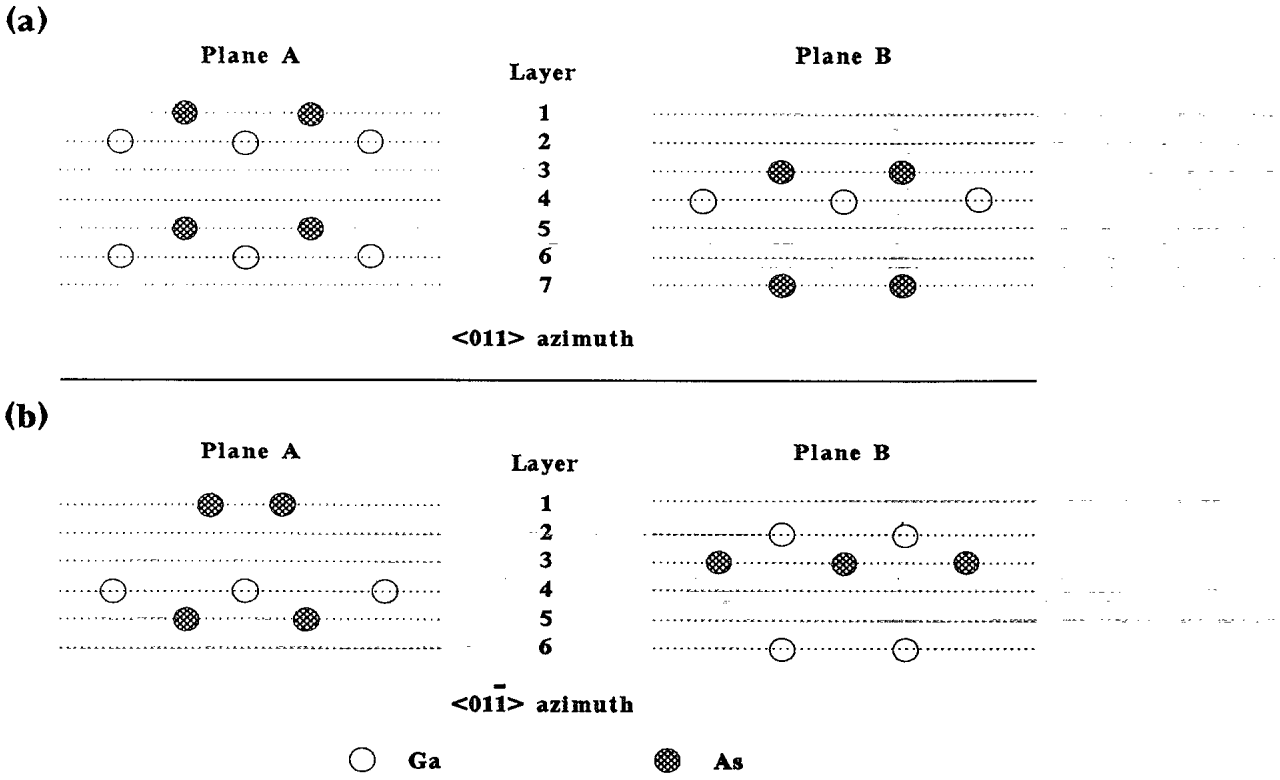

FIG. 3. Cross sections of the GaAs{001}(2×4) model surface indicating the atomic plane geometries parallel to the (a) ⟨011⟩ and (b) $\langle 01\bar{1} \rangle$ crystal directions.

Ar^+-ion bombardment of the dimer-reconstructed Si{001}(2×4) surface.[34,35] The Ar-Si interactions are described by pair potential.[36] The Si-Si interactions are described by using the Tersoff potential[37] for the attractive interaction, and the Molière potential for the very short-range repulsive interaction. In order to save computer time, a moving-atom approximation has been introduced into the calculation: instead of calculating the forces for all the atoms, only the equations of motion of the atoms which have been impacted are integrated.[24,36]

The Si{001}(2×4) crystal structure used in the calculation was composed of 2184 atoms distributed in ten layers. The first-layer atoms are dimerized with a bond length of 2.38 Å (the bulk distance is 3.84 Å). The positions of the atoms were determined by an energy-minimizing calculation with periodic-boundary conditions[38] in the two horizontal directions. The calculated ejected atom intensity, as a function of polar angle of incidence, is plotted in Fig. 4 for Ar incidence parallel to the $\langle 01\bar{1} \rangle$ (the dimer bond) direction. The data for each point on the plot was obtained by averaging 800 trajectories spread over the representative impact zone. For each collision process that results in the ejection of atoms from the surface, the initial positions, the final velocities and the identities of the ejected particles are stored for subsequent analysis. The time-dependent positions and velocities are monitored to determine collisional mechanisms. For this study, we are primarily interested in the collisional mechanisms of the intensity enhancement in the angular distribution. The microscopic mechanisms of ejection responsible for the intensity distribution have been determined by tracking the atomic motions. These calculations have been used to confirm the assignment of mechanisms responsible for features observed in the experimental results.

A detailed analysis of the particle trajectories indicates that when the incidence angle is 70° the increased secondary particle yield is due to an ejection mechanism where the incident particles are deflected by second-layer atoms and collide with the nearest atoms in the incident direction in the same layer. A similar mechanism causes the enhanced desorption at $\theta_i = 62°$, except that the particle beam is impacting first-layer atoms. For an unreconstructed surface the enhanced intensity from this mechanism would occur at about $\theta_i = 70°$, but the peak is shifted because of the dimer structure of the first-layer atoms parallel to the incident direction. There is no simple assignment for the smaller feature at $\theta_i = 45°$. The analysis indicates that this feature is caused by a combination of channeling and blocking effects. The high secondary yield at $\theta_i = 25°$ is almost entirely due to incident particles that are deflected by second-layer atoms, and then impact third-layer atoms. Finally, the mechanism responsible for the enhanced intensity at $\theta_i = 15°$ is incident par-

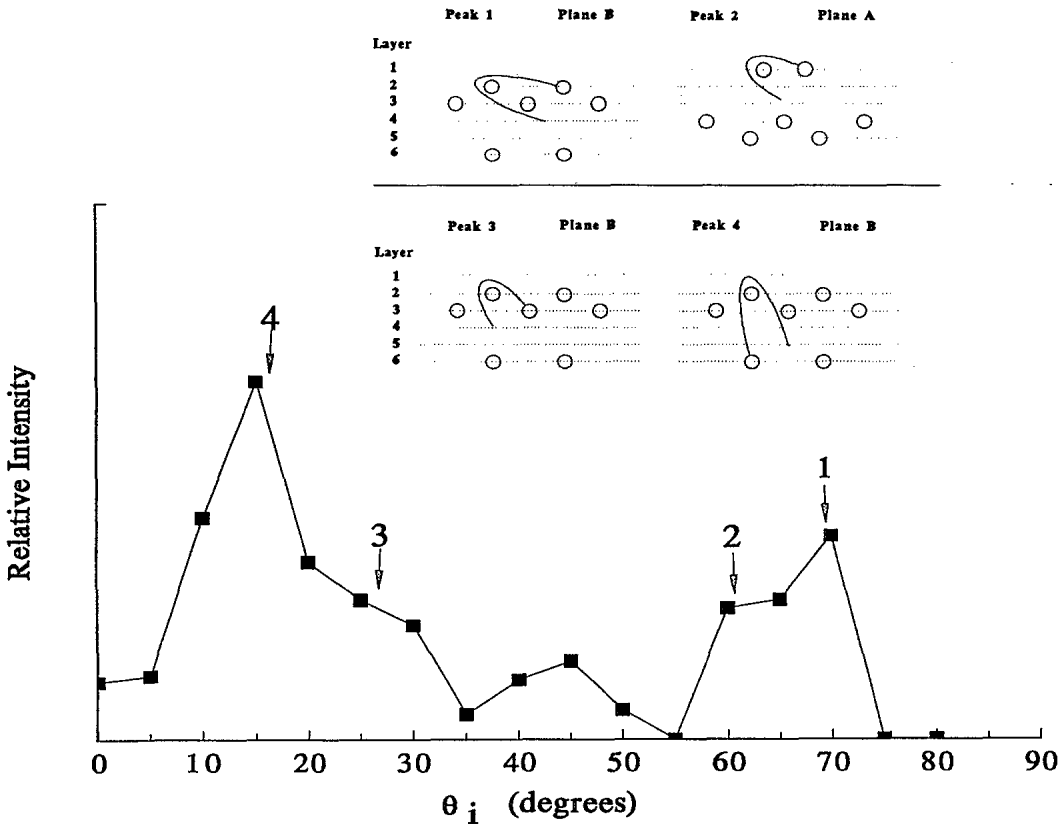

FIG. 4. Calculated intensity distribution, using molecular-dynamics simulations, of 10–100-eV Si atoms desorbed by 3-keV Ar bombardment of the Si{001}(2×4) surface. The desorbed Si intensity is plotted as a function of the incident-beam polar angle, relative to the surface normal. The beam is parallel to the $\langle 01\bar{1} \rangle$ crystal direction. The arrows refer to peak positions calculated using a two-body collision approximation.

ticle flux, focused by second-layer atoms, impinging on sixth-layer atoms (Fig. 4).

As discussed above, the molecular-dynamics calculation provides a rigorous basis for understanding the mechanisms of atom ejection due to keV particle bombardment for the open semiconductor surface. There are three factors, however, which hinder the general application of the molecular-dynamics calculation to the quantitative interpretation of the experimental data reported in this study. First, there is a lack of thorough understanding of the interaction potential for GaAs. Second, and most important, about 800 individual trajectories are required for each angle of incidence in the calculation in order to obtain a statistically valid result. Therefore, the calculation is time consuming. The last factor is that the molecular-dynamics calculation provides predictions for the yield of neutral atoms rather than for the yield of ionized species, which is experimentally measured.

A computationally less intensive approach has been used in the analysis of the experimental data. This approach consists of three basic steps. Step one involves the determination of the shadow-cone shape, using a two-body collision calculation with the Thomas-Fermi Molière potential. The Firsov screening factor required for this potential may be determined analytically or experimentally, and is discussed in detail in the next section. For GaAs, two shadow-cone shapes must be calculated, one for Ga and one for As, depending on which atom is creating the shadow cone. In step two of the analysis, the bulk structure is used to calculate the ion-incidence angles where the shadow-cone edge from a surface atom intersects other atomic positions. These calculated angles of incidence are correlated with enhanced intensity features of the experimental distribution in order to determine which of the features may be explained by

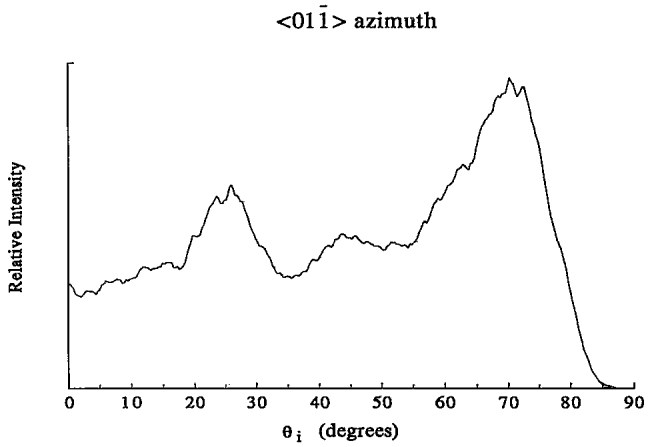

FIG. 5. The relative intensity of 20-eV Ga^+ ions desorbed from the GaAs{001}(2×4) surface by 3-keV Ar^+-ion bombardment, plotted as a function of the ion-beam polar angle, relative to the surface normal. The ion beam is parallel to the $\langle 01\bar{1} \rangle$ crystal direction.

desorption mechanisms involving atoms in GaAs bulk positions. For a reconstructed surface, such as GaAs{001}(2×4), many of the experimental features do not originate from these mechanisms. The third step in the analysis, therefore, involves varying the positions of the surface atoms in order to obtain a fit between the experimental and calculated incidence angles. This step proceeds until a self-consistent model of the surface structure is obtained.

The results obtained in two-body calculations were compared with those of molecular-dynamics simulations. The positions of enhanced-intensity features for the Si{001}(2×4) surface were determined using the two-

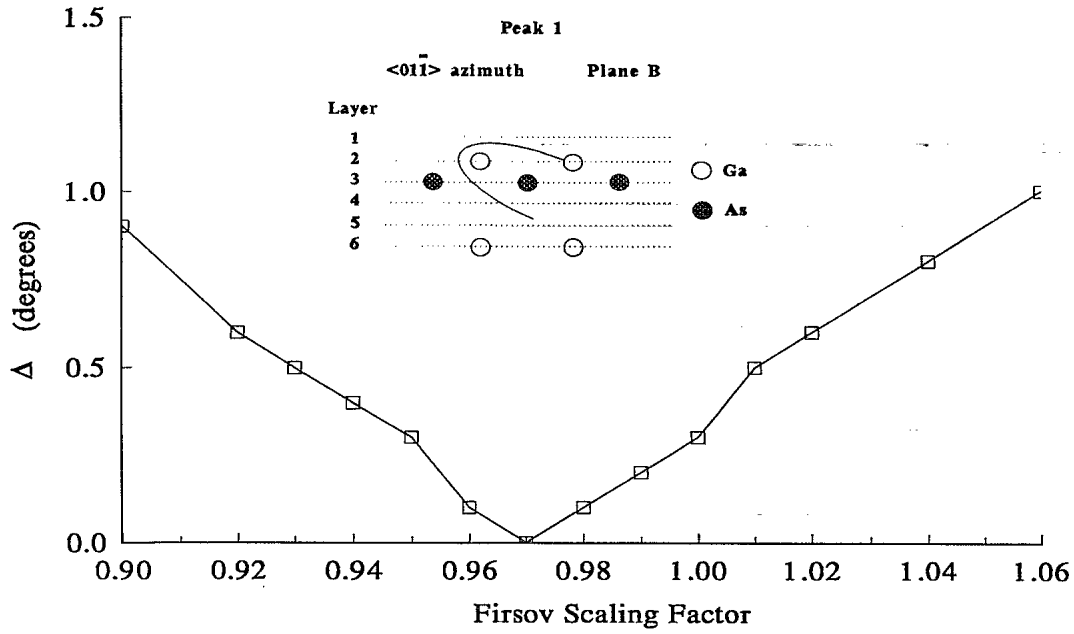

FIG. 6. The difference Δ between the experimental and calculated peak positions for the second-layer Ga-Ga atom interaction (peak 1), parallel to the $\langle 01\bar{1} \rangle$ crystal direction, plotted as a function of the Firsov scaling factor.

body approach. The angles of incidence for these features are represented by arrows in Fig. 4. The agreement between the two methods of calculation is excellent.

C. Shadow-cone-enhanced SIMS of GaAs{001}(2×4)

A typical shadow-cone-enhanced SIMS spectrum, taken parallel to the $\langle 01\bar{1}\rangle$ crystal direction of GaAs{001}(2×4) for an incident Ar^+-ion beam energy of 3 keV, is presented in Fig. 5. The signal intensity of desorbed secondary Ga^+ ions is plotted as a function of the polar angle of incidence θ_i of the ion beam relative to the surface normal. The experiment was performed with the detection angle β fixed at 21° relative to the ion beam. This angle represents the best compromise between high background signal at higher detection angles, and blocking effects at lower detection angles. The spectrum consists of four major peaks at polar angles of $\theta_i = 70.1°$, 63.0°, 44.5°, and 25.8°. Although there are some other distinguishable features in the spectra, no attempt was made to speculate upon their origins because of their poor reproducibility and low signal-to-noise level. In the analysis which follows, only reconstructions in the top two atomic layers are considered. Third- and deeper-layer atoms are assumed to be positioned in bulklike sites because experimental and theoretical studies indicate that atoms in these layers are unlikely to move more than 0.1 Å upon reconstruction of the surface.[39–41] The precision limit of our measurements is ±0.1 Å.

As discussed earlier in this paper, the Molière potential may be used in a simple two-body interaction calculation to analyze the data; however, the Firsov screening factor must first be determined. One method of doing this is to solve analytical approximations of the screening factor such as the following equation:[42]

$$f(Z_1,Z_2)=0.54+0.045[(Z_1)^{1/2}+(Z_2)^{1/2}] . \quad (1)$$

In this equation, Z_1 is the atomic number of the projectile and Z_2 is the atomic number of the target. For an Ar^+ ion interacting with a Ga surface atom, $Z_1=18$, $Z_2=31$, and $f=0.98$. Alternatively, the Firsov screening factor may also be determined experimentally, if the results of the two-body calculation can be compared with experimental data for an interaction between two atoms whose positions are known. Peak 1, at $\theta_i=70.1°$ in Fig. 5, represents just such a case. The peak arises from the shadow-cone interaction of two second-layer Ga atoms which are 4.0 Å apart, as shown in Fig. 3(b), plane B. The Ga atoms are assumed to be 4.0 Å apart because studies of semiconductor surface structure have not indicated large lateral displacements in the second atomic layer.[39–41] In Fig. 6 we present a difference function Δ (the difference of the experimentally determined peak position, 70.1°, from the peak position derived in the calculation) plotted versus the Firsov screening factor. The experimentally determined factor of 0.97 is in very close agreement with the factor of 0.98 determined from the Eq. (1).

Peak 2, at 63.0° in Fig. 5, corresponds to the shadow-cone interaction between the two atoms of the surface As_2 dimer shown in Fig. 2 (top view) and Fig. 3(b), plane A (side view). Using the experimental value of the Firsov screening factor determined previously, we present in Fig. 7 the peak difference function Δ between the experiment and calculation. Note that Δ is now plotted as a function of the As_2-dimer bond distance. The bond length is determined to be 2.73±0.10 Å.

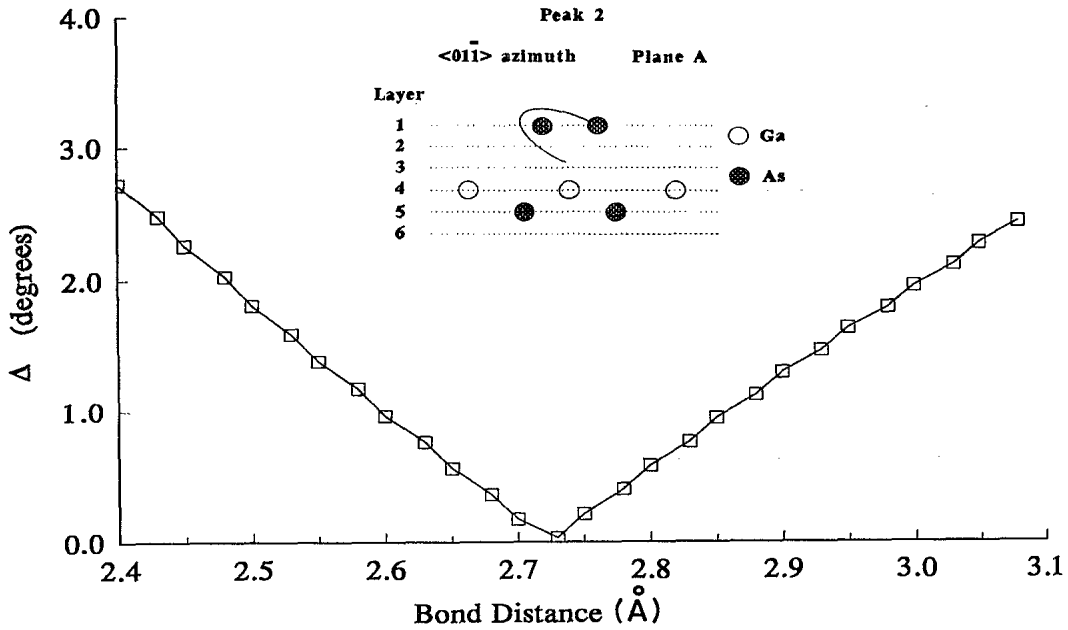

FIG. 7. The difference Δ between the experimental and calculated peak positions for the first-layer As-As dimer interaction (peak 2), parallel to the $\langle 01\bar{1}\rangle$ crystal direction, plotted as a function of the dimer bond distance.

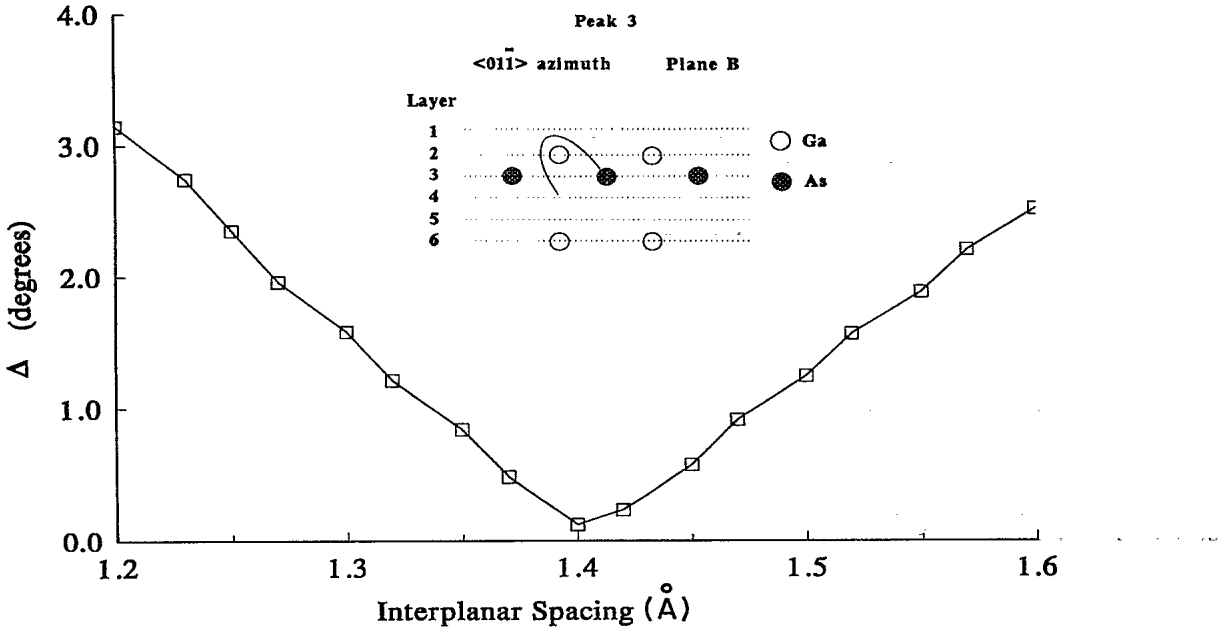

FIG. 8. The difference Δ between the experimental and calculated peak positions for the second-layer Ga to third-layer As interaction (peak 3), parallel to the $\langle 01\bar{1} \rangle$ crystal direction, plotted as a function of the interlayer spacing.

Peak 3, at $\theta_i = 25.8°$ in the shadow-cone-enhanced SIMS spectrum taken parallel to the $\langle 01\bar{1} \rangle$ crystal direction of the GaAs{001}(2×4) surface, shown in Fig. 5, arises from an interaction mechanism in plane B of Fig. 3(b). Specifically, the shadow-cone edge, produced by the incident ion collisions with the second-layer Ga atoms, coincides with the atomic position of the third-layer As atom at a polar angle of 25.8°. In this case the peak difference Δ can be plotted as a function of the interplanar spacing between the second and third planes, as shown in Fig. 8. The experimentally determined value is 1.40±0.10 Å, in agreement with the bulk-crystal value of 1.41 Å.

The shadow-cone-enhanced SIMS spectrum taken parallel to the $\langle 011 \rangle$ crystal direction of GaAs{001}(2×4) surface is shown in Fig. 9. The detection angle β is again fixed at 21°, and this experiment is therefore the analog of the one presented in Fig. 5, except that the crystal has been rotated azimuthally by 90°. In this direction, the signal intensity should represent ion-atom interactions in the two planes of Fig. 3(a). The spectrum is dominated by a single peak at a polar angle of $\theta_i = 25.3°$. which arises from shadow-cone interactions between the third-layer As atoms and fourth-layer Ga atoms [Fig. 3(a), plane B]. As it is very reasonable to assume that there is no significant reconstruction of the surface in these layers, this peak provides an excellent means of checking the value of the Firsov screening factor determined earlier. The experimentally determined value for the interplanar spacing is 1.43±0.10 Å, in close agreement with the bulk-crystal spacing of 1.41 Å. This again indicates that the Firsov screening factor used in these calculations is reasonable. The peak at 25.3° in Fig. 9 corresponds well with the peak at 25.8° in Fig. 5, as it should since the two interaction mechanisms responsible for the peaks are very similar.

As a final means of testing this shadow-cone-enhanced SIMS analysis of the GaAs{001}(2×4) surface, the experiment was repeated parallel to the $\langle 01\bar{1} \rangle$ crystal direction, which contains the important As_2-dimer bond information. In this experiment, however, the detector was no longer maintained at a fixed position relative to the ion beam. Instead, the detector was stepped in the polar plane (the horizontal plane in Fig. 1) synchronously with the sample such that the detector was always parallel to the surface normal. The goal of this experiment is to eliminate possible distortions to the shadow-cone-enhanced SIMS spectrum intensity which might arise

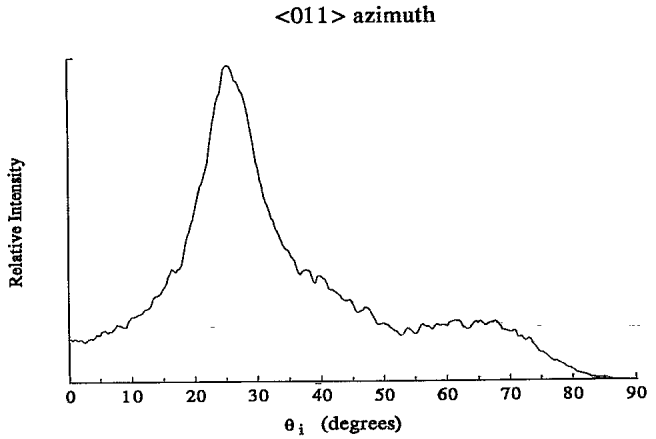

FIG. 9. The relative intensity of 20-eV Ga^+ ions desorbed from the GaAs{001}(2×4) surface by 3-keV Ar^+-ion bombardment, plotted as a function of the ion-beam polar angle relative to the surface normal. The ion beam is parallel to the $\langle 011 \rangle$ crystal direction.

from blocking and direct ejection mechanisms involving secondary Ga^+ ions. These mechanisms have been analyzed in detail in angle-resolved SIMS studies of the GaAs{001}(2×4) surface.[33] The shadow-cone-enhanced SIMS spectrum using this alternate method is shown in Fig. 10, which should be compared with the spectrum shown in Fig. 5. The four peaks are still very much in evidence.

The information contained in the spectrum shown in Fig. 10 has several implications. First, the spectrum is extremely similar to the one presented in Fig. 5, indicating that the peaks have been correctly assigned as shadow-cone interactions and are not the result of secondary-ion-surface mechanisms such as blocking, channeling, direct ejection along a bond axis, etc. Secondly, the shadow-cone intensity peaks are superimposed on a signal background which *does* include secondary-ion blocking and channeling effects as well as other unassigned mechanisms; this implies that the intensity of the shadow-cone peaks may be unreliable as measures, and only the peak positions should be used for data analysis. Lastly, the peak positions can be slightly influenced by the presence of secondary-ion ejection mechanisms. The peak associated with the second-layer Ga-Ga interaction has shifted from 70.1° to 68°. The peak associated with the As-As-dimer interaction has shifted from 63° to 61°. The peak positioned at 25.8° remains constant in the two methods. If the peak at 68° is now used to calibrate the shadow cone, the peak at 61° represents an As-As-dimer bond length of 2.8 Å. It is, therefore, this secondary-ion-surface interaction which presently constrains the final precision of the measurements to ±0.10 Å. (The experimental precision is better than ±0.05 Å.)

A summary of the analysis is presented in Table I. There are two factors which need to be addressed concerning the reliability of these results. All of the angles where the focused ion flux interacts with an atom have been assigned from the local maximum of the peaks. There are other ways to define the intersect position of the shadow-cone tail with a neighboring atom.[43,44] Our method is based on three-dimensional molecular-dynamics calculations, which are the foundation of the ion-atom interaction analysis used in this paper. This method has been used successfully in other shadow-cone-enhanced SIMS studies.[27,31] Also, the shadow-cone shape used in this analysis has been calibrated experimentally and is in agreement with the empirical calculation of the Firsov screening factor. To avoid false assignment of the interaction mechanisms, all possible combinations of assignments that can yield the features observed experimentally have been analyzed.

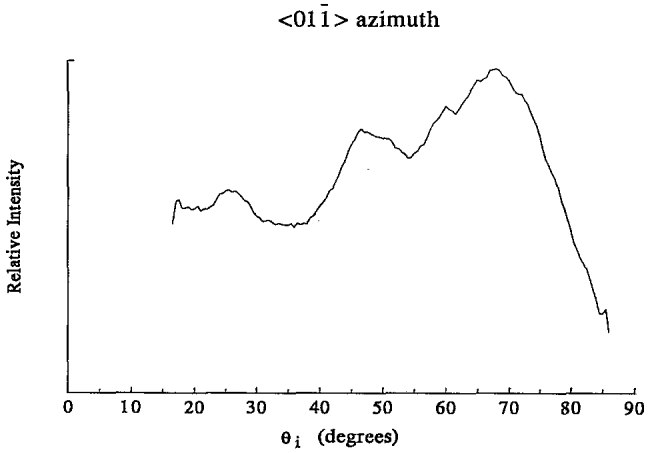

FIG. 10. The relative intensity of 20-eV Ga^+-ions desorbed from the GaAs{001}(2×4) surface by 3-keV Ar^+-ion bombardment, plotted as a function of the ion-beam polar angle, relative to the surface normal. The ion beam is parallel to the ⟨01$\bar{1}$⟩ crystal direction, and the detector is maintained parallel to the surface normal in this experiment.

The experimental As_2-dimer bond distance of 2.73 Å is expanded slightly from the bond distance of 2.51 Å found on bulk As where there is threefold coordination,[45] but is substantially larger than the average tetrahedral covalent bond distance for As of 2.36 Å.[46] The larger dimer bond length, relative to the covalent bonds, may indicate that the atoms of the As_2 dimer are threefold coordinated, as they are in bulk As. Instead of the tetrahedral sp^3 hybridized bonding of As in the GaAs lattice, the As dimers have the As 4*s* state split from the 4*p* states. In this configuration, the 4*p* orbitals form the dimer bonds and backbonds to the substrate, while the 4*s* orbital becomes the filled, non-bonding orbital. Threefold coordination of the As reduces the backbonding strain of the system, stabilizing the surface. The different chemical nature of threefold-coordinated As also has implications in growth models of GaAs.[2,47] Theoretical studies of GaAs{001}, using threefold-coordinated orbital configurations for surface As (which result in a dimer bond distance of 2.5±0.05 Å), have been very successful at modeling the (2×4) surface and at identifying dimer-induced surface electronic states in the band structure.[14,39,48,13] In the case of As dimers on Si{001}, *ab initio* pseudopotential

TABLE I. Experimental and calculated results. The distances are in unit of angstroms and the angles are expressed in degrees. D_{11} is the first-layer As-As bond distance in a ⟨01$\bar{1}$⟩ direction; D_{22} the second-layer Ga-Ga distance along a ⟨01$\bar{1}$⟩ direction; D_{23} the interplanar distance between the second and third layer; D_{34} the interplanar distance between the third and fourth layer.

Cryst. direction	Peak	θ_i	D_{bulk}	D_{anal}	D
⟨01$\bar{1}$⟩	Peak 1	70.1	4.00	4.00±0.10	D_{22}
	Peak 2	63.0	4.00	2.73±0.10	D_{11}
	Peak 3	25.8	1.41	1.40±0.10	D_{23}
⟨011⟩	Peak 1	25.3	1.41	1.43±0.10	D_{34}

calculations assuming threefold-coordinated As have replicated the surface band structure of the system almost exactly, including gap electronic states.[40]

The As-As-dimer bond distance of 2.73±0.10 Å determined in this work is within experimental error of the As-As-dimer bond distance of 2.59±0.06 Å reported in a grazing-incidence x-ray diffraction study of the GaAs{001}$c(4\times4)$ surface.[18] It is also very close to an As-As-dimer bond distance of 2.55 Å reported for As adsorbed onto the Si{001}(2×1) surface.[40] In all three cases, the dimer bond distance is much closer to the bulk As bond distance, with threefold coordination, than to the tetrahedral covalent As bond distance. Further evidence for this interpretation is provided by a recent surface-extended x-ray-absorption fine structure/STM study which found the Sb-Sb-dimer bond distance on Si{001}(2×1)-Sb to be 2.88±0.03 Å.[49] This is very close to the bulk value of threefold-coordinated Sb of 2.90 Å.[45]

The only other reported value of the As-As-dimer bond distance on the GaAs{001}(2×4) surface is 2.2 Å.[15] This bond length is close to the gas-phase As_2 bond distance of 2.1 Å.[50] A bond length this short would seem to imply that the As_2 dimer is very weakly bound to the surface, or else a large amount of backbonding strain in the system would result. It was suggested that perhaps the As_2 dimers are "buckled," which could allow the determined bond distance to approach the tetrahedral covalent bond distance of 2.36 Å; however, current theoretical studies do not seem to support a buckled-dimer model of the surface.[14,39,40,13]

IV. CONCLUSION

We have used shadow-cone-enhanced SIMS experiments to verify the presence of As-As dimer bonds in the top layer of the GaAs{001}(2×4) surface reconstruction. The dimer bond length was determined to be 2.73±0.10 Å, and there was no indication of the dimers tilting out of the plane of the surface. Within the precision of the measurements, no relaxation effects were displayed in the second and lower layers of the surface.

Shadow-cone-enhanced SIMS is an effective tool in the analysis of surface atomic geometries. While the technique is based upon a solid foundation of scattering theory and molecular-dynamics simulations, the calculations for a specific experiment are straightforward and require very little computation. The precision of the measurements should improve with further experimental and theoretical refinements.

ACKNOWLEDGMENTS

The authors appreciate many helpful discussions with R. Blumenthal, E. Furman, S. Donner, and J. O'Connor. This work was partially supported by funds from the National Science Foundation and the Office of Naval Research. The Pennsylvania State University supplied a generous grant of computer time for these studies. One of us (B.J.G.) gratefully acknowledges partial support by the Camille and Henry Dreyfus Foundation.

[1]T.-C. Chiang, R. Ludeke, M. Aono, G. Landgren, F. J. Himpsel, and D. E. Eastman, Phys. Rev. B **27**, 4770 (1982).
[2]H. H. Farrell, J. P. Harbison, and L. D. Peterson, J. Vac. Sci. Technol. B **5**, 1482 (1987).
[3]M. D. Pashley, K. W. Habereen, W. Friday, J. M. Woodall, and P. D. Kirchner, Phys. Rev. Lett. **60**, 2176 (1988).
[4]W. E. Spicer, I. Lindau, P. Skeath, C. Y. Su, and P. Chye, Phys. Rev. Lett. **44**, 420 (1980).
[5]S. A. Chambers, Phys. Rev. B **39**, 12 664 (1989).
[6]A. Y. Cho, J. Appl. Phys. **41**, 2780 (1970).
[7]J. R. Arthur, Surf. Sci. **43**, 449 (1974).
[8]J. H. Neave and B. A. Joyce, J. Cryst. Growth **44**, 387 (1978).
[9]P. Drathen, W. Ranke, and K. Jacobi, Surf. Sci. **77**, L162 (1978).
[10]S. P. Svensson, P. O. Nilsson, and T. G. Andersson, Phys. Rev. B **31**, 5272 (1985).
[11]R. Z. Bachrach, R. S. Bauer, P. Chiaradia, and G. V. Hansson, J. Vac. Sci. Technol. **18**, 797 (1981).
[12]P. K. Larsen, J. H. Neave, J. F. van der Veen, P. J. Dobson, and B. A. Joyce, Phys. Rev. B **27**, 4966 (1983).
[13]D. J. Chadi, J. Vac. Sci. Technol. A **5**, 834 (1987).
[14]P. K. Larsen and D. J. Chadi, Phys. Rev. B **37**, 8282 (1988).
[15]S. A. Chambers, Surf. Sci. **248**, L274 (1991).
[16]D. K. Biegelsen, R. D. Bringans, J. E. Northrup, and L.-E. Swartz, Phys. Rev. B **41**, 5701 (1990).
[17]M. Sauvage-Simkin, R. Pinchaux, J. Massies, P. Calverie, J. Bonnet, N. Jedrecy, and I. K. Robinson, Surf. Sci. **211/212**, 39 (1989).
[18]M. Sauvage-Simkin, R. Pinchaux, J. Massies, P. Calverie, N. Jedrecy, J. Bonnet, and I. K. Robinson, Phys. Rev. Lett. **62**, 563 (1989).
[19]J. F. van der Veen, Surf. Sci. Rep. **5**, 199 (1985).
[20]E. S. Mashkova and V. A. Molchanov, Radiat. Eff. **19**, 29 (1973).
[21]E. S. Mashkova and V. A. Molchanov, Radiat. Eff. **23**, 215 (1974).
[22]M. Kato, M. Katayama, T. Chasse, and M. Aono, Nucl. Instrum. Methods B **39**, 30 (1989).
[23]C.-C. Chang, Ph.D. thesis, Pennsylvania State University, 1987.
[24]R. Smith, D. E. Harrison, Jr., and B. J. Garrison, Phys. Rev. B **40**, 93 (1989).
[25]R. Smith, D. E. Harrison, Jr., and B. J. Garrison, Nucl. Instrum. Methods B **46**, 1 (1990).
[26]B. J. Garrison, N. Winograd, D. M. Deaven, C. T. Reimann, D. Y. Lo, T. A. Tombrello, D. E. Harrison, Jr., and M. H. Shapiro, Phys. Rev. B **37**, 7197 (1988).
[27]C.-C. Chang and N. Winograd, Phys. Rev. B **39**, 3467 (1989).
[28]C.-C. Chang, Surf. Interface Anal. **15**, 79 (1990).
[29]N. Winograd and C.-C. Chang, Phys. Rev. Lett. **62**, 2568 (1989).
[30]C.-C. Chang and N. Winograd, Surf. Sci. **230**, 27 (1990).
[31]R. Blumenthal, S. K. Donner, J. L. Herman, R. Trehan, K. P. Caffey, E. Furman, N. Winograd, and B. D. Weaver, J. Vac. Sci. Technol. B **6**, 1444 (1988).
[32]K. Caffey, R. Blumenthal, J. Burnham, E. Furman, and N.

Winograd, J. Vac. Sci. Technol. B **9**, 2268 (1991).
[33]R. Blumenthal, K. P. Caffey, E. Furman, B. J. Garrison, and N. Winograd, Phys. Rev. B **44**, 12 830 (1991).
[34]E. Kaxiras and K. C. Pandey, Phys. Rev. B **38**, 12 736 (1988).
[35]B. W. Dodson, Phys. Rev. B **35**, 2795 (1987).
[36]D. E. Harrison, Jr., Crit. Rev. Solid State Mater. Sci. **14**, S1 (1988).
[37]J. Tersoff, Phys. Rev. B **37**, 6991 (1988).
[38]D. W. Brenner and B. J. Garrison, *Advances in Chemical Physics Molecule Surface Interactions,* edited by K. P. Lawley (Wiley, New York, 1989), p. 281.
[39]G.-X. Qian, R. M. Martin, and D. J. Chadi, Phys. Rev. Lett. **60**, 1962 (1988).
[40]R. I. G. Uhrberg, R. D. Bringans, R. Z. Bachrach, and J. E. Northrup, Phys. Rev. Lett. **56**, 520 (1986).
[41]G. A. Somorjai, *Chemistry in Two Dimensions: Surfaces* (Cornell University Press, London, 1981), p. 148.
[42]D. J. O'Connor and R. J. MacDonald, Radiat. Eff. **34**, 247 (1977).
[43]M. Aono, C. Oshima, S. Zaima, S. Otani, and Y. Ishizawa, Jpn. J. Appl. Phys. **20**, L829 (1981).
[44]M. Aono, Y. Hou, R. Souda, C. Oshima, S. Otani, Y. Ishizawa, K. Matsuda, and R. Shimizu, Jpn. J. Appl. Phys. **21**, L670 (1982).
[45]N. N. Greenwood and A. Earnshaw, *Chemistry of the Elements* (Pergamon, New York, 1984), p. 643.
[46]C. Kittel, *Introduction to Solid State Physics,* 6th ed. (Wiley, New York, 1986), p. 76.
[47]D. J. Frankel, C. Yu, J. P. Harbison, and H. H. Farrell, J. Vac. Sci. Technol. B **5**, 1113 (1987).
[48]P. K. Larsen, J. F. van der Veen, A Mazur, J. Pollmann, J. H. Neave, and B. A. Joyce, Phys. Rev. B **26**, 3222 (1982).
[49]M. Richter, J. C. Woicik, J. Nogami, P. Pianetta, K. E. Miyano, A. A. Baski, T. Kendelewicz, C. E. Bouldin, W. E. Spicer, C. F. Quate, and I. Lindau, Phys. Rev. Lett. **65**, 3417 (1990).
[50]K. P. Huber and G. Herzberg, *Molecular Spectra and Molecular Structure, Vol. 4* (Van Nostrand Reinhold, New York, 1979), p. 38.